

Displacement of CO₂ by Xe in single-walled carbon nanotube bundles

Christopher Matranga,^{1,*} Liang Chen,^{1,2} Bradley Bockrath,¹ and J. Karl Johnson^{1,2}

¹*National Energy Technology Laboratory, United States Department of Energy, Pittsburgh, Pennsylvania 15236, USA*

²*Department of Chemical and Petroleum Engineering, University of Pittsburgh, Pittsburgh, Pennsylvania 15261, USA*

(Received 20 April 2004; published 22 October 2004)

The displacement of CO₂ by Xe on single-walled nanotube bundles is investigated with Fourier transform infrared spectroscopy (FTIR) and grand canonical Monte Carlo (GCMC) simulations. The FTIR experiments show that CO₂ physisorption at 77 K produces an infrared peak at 2330 cm⁻¹ for endohedral physisorption and at 2340 cm⁻¹ for groove/external surface physisorption. Exposure to Xe causes a sequential displacement of CO₂ from these sites as shown by an intensity loss of the 2330 cm⁻¹ peak, which precedes the loss at 2340 cm⁻¹. The GCMC simulations on heterogeneous and homogenous bundles show that CO₂ in endohedral sites is initially displaced by Xe before that in groove/external surface sites. The CO₂ populations in each site of the bundle are taken from the GCMC simulations and used to model the variation of the FTIR intensities as a function of Xe pressure. The qualitative agreement between the simulated and experimental intensity changes is good, suggesting that the intensity changes seen in the experiments are related to CO₂ displacement from the sites indicated in the simulations.

DOI: 10.1103/PhysRevB.70.165416

PACS number(s): 61.46.+w, 68.43.Fg, 68.43.Pq, 78.30.Na

I. INTRODUCTION

Studying how gases physisorb on single-walled carbon nanotube bundles (SWNTs) not only yields information about the interactions of gases with these materials but can also produce fruitful information about the bundle itself. Knowledge of how gases access endohedral and interstitial sites aids our understanding of the defects present along nanotube sidewalls and on how these nanotubes have crystallized to form bundles. The effects that common purification steps have on access to these sites add another dimension of understanding, because acid oxidation can block sites through the addition of functionalization.

Molecular vibrations are sensitive to their local environment, so infrared studies are useful for differentiating molecules in samples with multiple adsorption sites.¹⁻⁶ In this regard, CO₂ is an obvious choice for a probe molecule since its ν_3 asymmetric stretch mode has a large infrared cross section, making it easily detectable with a standard FTIR spectrometer. In fact, several experimental and computational studies have appeared for CO₂ adsorption in SWNTs, so a fair amount of data exists for this system.^{3,4,7-11}

Here, we present a joint experimental and computational study on the displacement of CO₂ by Xe in acid purified SWNTs. Both the experiments and simulations show there is a sequential displacement of physisorbed CO₂ by Xe with endohedral and interstitial sites preceding groove/external surface sites. Data from the molecular simulations are used to model how the experimental IR intensities should vary during displacement assuming Lorentzian lineshapes with spectroscopic parameters for each site set from previous experiments.^{3,4,7} The qualitative agreement between these simulated IR spectra and the actual IR experiments is good, suggesting that the sites associated with the IR peak assignments and their intensity variations are adequately represented by the system used in the molecular simulations.

II. METHODS

A. Experimental

Infrared studies in the transmission geometry were performed in a vacuum chamber described previously.⁴ The SWNT sample was purchased from Tubes@Rice as a "Purified Grade" suspended in toluene. This sample was produced by the laser ablation technique followed by acid purification.¹²⁻¹⁴ Infrared samples were thin films prepared by dispersing the sample directly on a 1 mm thick plane parallel CaF₂ window (Janos Technology) and evaporating the solvent in a 120 °C oven for ~5 min. The background absorption of the film was adjusted by adding sample until the film had an optical density of ~0.9 near 2300 cm⁻¹. This film thickness gave enough sample path length to allow the observation of physisorbed CO₂ under the pressures and temperatures accessed in this study. Samples were degassed in the vacuum chamber at 373 K for 2 h prior to use. CO₂ was physisorbed on the sample at 77 K by closing the gate valve between the pumping system and the chamber and backfilling the cell to a static pressure. All reported experimental pressures are uncorrected ion gauge values determined in the main portion of the chamber. After the infrared intensity growth from CO₂ physisorption was saturated with respect to pressure, Xe displacement studies were run by back filling the chamber with Xe to a desired pressure. To test that we were observing equilibrium conditions for the displacement of CO₂ we (i) heat the sample to 300 K (gate valve still closed) after reaching the highest experimental pressure ($P_{\text{Xe}} + P_{\text{CO}_2} \sim 0.8$ mTorr); (ii) check with IR that CO₂ is completely desorbed from the sample; and (iii) quench the sample back to 77 K. The cell pressure and the integrated intensity for physisorbed CO₂ return to within ~5% and ~15%, respectively, of their values before heating. Furthermore, we see no redistribution of CO₂ intensities from the IR peaks associated with the different adsorption sites.

TABLE I. Classes of Nanotube bundles studied in the molecular simulations in this work. The diameters are 10.84, 12.20, 13.56, 14.92, and 16.28 Å for the (8,8) through (12,12) nanotubes.

Bundle	No. of (8,8) tubes	No. of (9,9) tubes	No. of (10,10) tubes	No. of (11,11) tubes	No. of (12,12) tubes	Average diameter (Å)
1	2	2	10	2	2	13.56
2	3	5	12	3	2	13.54
3	0	0	16	0	0	13.56

B. Computational

Adsorption isotherms were computed from grand canonical Monte Carlo (GCMC) simulations.¹⁵ The GCMC algorithm consists of three types of moves, namely, translation and rotation of a single molecule, creation of a new molecule, and deletion of an existing molecule. Moves were attempted randomly with a 20% probability for translation/rotation and 40% each for creation and deletion. Simulations were typically equilibrated for 5×10^7 moves, followed by data taken for 10^7 moves. The maximum displacement step size was adjusted during equilibration to achieve approximately a 50% acceptance ratio for combined translation and rotation moves. Canonical simulations were used to calculate average energies at a fixed coverage.

The Xe–Xe interaction was modeled as a Lennard-Jones (LJ) potential. The parameters ($\sigma=4.1$ Å, $\epsilon/k=221$ K) were taken from the literature.¹⁶ The CO₂ and nanotube (carbon) potentials used in this work are the same as that used in our previous work.⁴ The CO₂–CO₂ potential was taken from Harris and Yung and includes effective charges to account for the quadrupole moment.¹⁷ The carbon atoms in the nanotube were assumed to have the same potential as carbons in a graphene sheet, with LJ parameters for carbon taken from Steele.¹⁸ Cross interactions were computed from the Lorentz–Berthelot combining rules. We have ignored any charge-related interactions between CO₂ and Xe or nanotubes (such as charge-induced dipole).

We have simulated adsorption and displacement on three different nanotube bundles. Two of the bundles are heterogeneous, i.e., composed of SWNTs of different diameters. The heterogeneous bundles contain packing defects that create large interstitial channels, capable of adsorbing both Xe and CO₂. These bundles are similar to those studied by Shi and Johnson.¹⁹ The third bundle is homogeneous, composed of only (10,10) SWNTs. The first bundle contains 18 SWNTs, ranging in size from 10.84 to 16.28 Å in diameter. The second bundle contains 25 SWNTs covering the same range of sizes. The homogeneous bundle contains 16 nanotubes. Details of the bundles, including the number of each type of nanotube, are given in Table I. The simulation code includes an algorithm for identifying molecules as being adsorbed in endohedral, interstitial, or external sites. This allows for accurate statistics on the occupation and energetics in these three classes of sites. By conducting simulations on bundles with different packing arrangements, we are able to show that the effects seen are general and not specific to a particu-

lar bundle arrangement. A more detailed description of the potential models and construction of nanotube bundles can be found in Ref. 4.

Spectral simulations were constructed by summing three Lorentzians to produce a lineshape representing the endohedral, interstitial, and groove/external surface sites in the bundle. The frequencies and full width half maximums (FWHMs) for each adsorption site were determined from tentative assignments made in previous experiments and remained fixed during the simulation at 2330 and 10 cm⁻¹, respectively, for endohedral sites; 2339 and 14 cm⁻¹, respectively, for interstitial sites; and 2340 and 20 cm⁻¹, respectively, for groove sites.^{3,4} As discussed below, the CO₂ populations for interstitial and groove/external surface sites are displaced by Xe over different pressure ranges, so including a Lorentzian near 2340 cm⁻¹ for both these sites can allow us to differentiate between them by examining the intensity profile near 2340 cm⁻¹ with pressure. The integrated intensity of the Lorentzian for each site in the bundle is set from their CO₂ populations at each pressure, which are extracted directly from the GCMC simulations.

Experiments indicate that the sample degassed at 373 K retains most of its functionality and, as a result, only has a small fraction of its endohedral and interstitial sites open to gas phase molecules. To account for this in the spectral simulations we multiply the GCMC determined CO₂ populations for the endohedral and interstitial sites of a fully open heterogeneous bundle by 0.05 to simulate how the spectra of a partially opened bundle might behave. The value of 0.05 gave a better “fit to eye” when compared to experimental spectra than values of 0.10, 0.15, or 0.20. We do not expect quantitative agreement between the spectral simulations and experiments (see discussion below), so these scaling factors are only used to easily simulate how selectively blocking an arbitrary fraction of endohedral/interstitial sites might change the spectral simulations when compared to simulations done on a fully open bundle without any such scaling. These scaling factors should not be interpreted, in any way, as being a quantitative representation of how many endohedral sites are opened/closed in the experimental system. The precise number of opened or closed sites cannot be obtained by the measurements presented here.

The experiments on the samples that were heated to 700 K indicate that many of the functionalities have been removed and, as a result, most of the adsorption sites in the bundle are accessible. Spectra for these samples are simulated by directly using the GCMC populations for a completely open, heterogeneous bundle without any scaling.

III. RESULTS AND DISCUSSION

A. Physisorption of CO₂

The physisorption of gas phase CO₂ on the SWNTs after vacuum degassing at 373 K is shown in Fig. 1. A single peak is seen at 2340 cm⁻¹ from the ν_3 mode of physisorbed CO₂ that gains intensity with pressure until beginning to saturate at about 5×10^{-7} Torr. The peak at 2340 cm⁻¹ on the acid oxidized SWNTs has previously been assigned to CO₂ physisorbed in groove sites on the periphery of the bundle.⁴ The

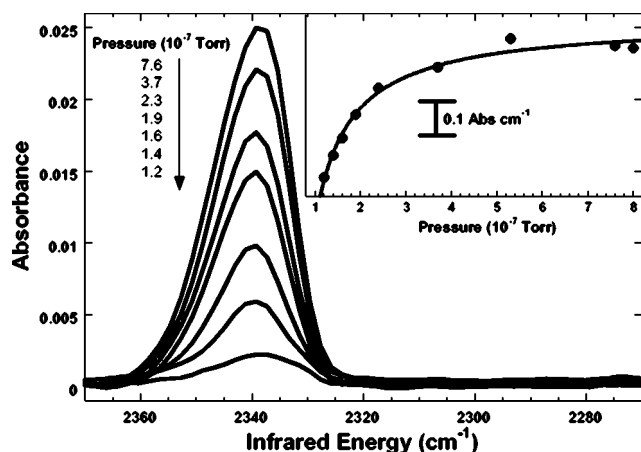


FIG. 1. Infrared spectra of CO₂ physisorbed on the SWNTs at 77 K after degassing at 373 K for 2 h. A single peak is seen near 2340 cm⁻¹ from the ν_3 mode of CO₂, which gains intensity with pressure. The inset shows the integrated intensity of the IR spectra from the main figure. The solid line in the inset is only meant as a guide to the eye. The inset shows that the integrated intensity of the IR peak starts to saturate at around 4×10^{-7} Torr, indicating a filling of sites associated with the 2340 cm⁻¹ peak.

SWNTs used in Fig. 1 have functionalities at defect sites from the acid purification step that can inhibit access to the endohedral and interstitial sites of the bundle.²⁰ Degassing at 373 K is not sufficient to cause the complete decomposition of these functionalities and consequently the IR spectra of Fig. 1 mostly show evidence for groove/external surface site adsorption.^{4,21} Later, we will show that there is some evidence from the Xe displacement studies that a small amount of endohedral adsorption does occur.

Vacuum heating of this sample to 700 K causes a partial decomposition of the functional groups that block access to the endohedral and interstitial sites of the bundle. The IR spectra associated with functionality decomposition on the sample used in this paper have been reported.⁴ Some of the CO₂ generated during decomposition becomes permanently entrapped in the SWNT bundle and has been studied previously.^{4,7}

In order to illustrate how vacuum heating removes functionalities and opens access to new adsorption sites, we examine the physisorption of CO₂ on the SWNTs after heating to 700 K (Fig. 2). Some intensity is seen at 2330 and 2340 cm⁻¹ due to the entrapped CO₂ present before introducing gas phase CO₂ to the cell.⁴ Physisorption of gas phase CO₂ first causes the shoulder at 2340 cm⁻¹ to gain intensity, with the peak at 2330 cm⁻¹ following. The peak at 2330 cm⁻¹ has been attributed to CO₂ in endohedral sites.^{3,4} The peak near 2340 cm⁻¹ is more ambiguous and is seen for both interstitial and groove sites.^{3,4,7} The similar ν_3 frequency seen for CO₂ in groove and interstitial sites suggests they have comparable adsorption environments. We have previously argued that the V-shaped pores created by adjacent nanotubes in large interstitial and groove sites are responsible for this environment.^{4,7} The reason for the similar morphology in the IR spectra for the trapped and physisorbed CO₂ has also been discussed.^{4,7}

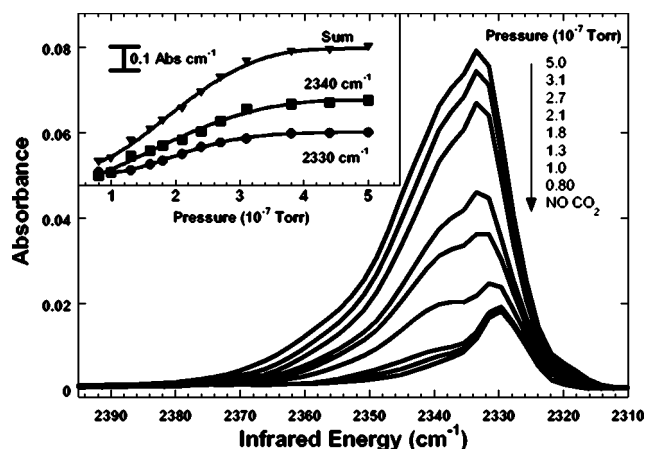


FIG. 2. Infrared spectra of CO₂ physisorbed on the SWNTs at 77 K after vacuum heating to 700 K. Peaks at 2330 and 2340 cm⁻¹ are seen before any gas phase CO₂ is introduced to the cell. These peaks are due to the physical entrapment of CO₂ in the bundle during the vacuum heating step. The inset shows the integrated intensity of 2330 cm⁻¹ (solid circles), 2340 cm⁻¹ (open squares), and their sum (solid triangles) as determined by deconvoluting the spectra from the main figure with a two Lorentzian fit.

B. Xe displacement of CO₂

Xe is a useful species for displacing molecules from SWNTs and this motivates our use of this technique to further understand CO₂ interactions with these materials.¹⁻³ Figure 3 shows simulation results for the displacement of CO₂ by Xe on three different nanotube bundles. The similarity of the displacement of CO₂ from the endohedral and groove/external surface sites in these three panels indicates that the general displacement behavior for these sites is independent of the type of bundle chosen for the simulation and therefore not model dependent. One notable difference in Fig. 3 is the complete lack of interstitial site access in the homogeneous (10, 10) bundle (bottom panel) because these sites are too small to accommodate CO₂. In the more realistic heterogeneous bundles (top two panels), some interstitial sites are accessible, but their populations make a small contribution to the total amount of adsorbed/displaced CO₂ (see discussion below). The lack of interstitial access in the homogeneous (10, 10) bundle is not necessarily what we expect to see experimentally, since this homogeneous bundle is not a realistic representation of the distribution of tubes known to make up actual nanotube samples. The results for the (10, 10) bundle are included in Fig. 3 mainly to illustrate that groove/external surface and endohedral site behavior is not sensitive to whether a heterogeneous or homogeneous bundle is used for the simulations.

For further discussion, we refer specifically to the results displayed in the top panel of Fig. 3 for a heterogeneous bundle (bundle 1 of Table I). The endohedral and interstitial sites of this bundle show a rapid loss of CO₂ in the presence of Xe with each site losing about $\frac{1}{2}$ of its initial CO₂ population by 1.7×10^{-6} Torr. The remaining fraction in these sites decreases by less than 10% between 1.7×10^{-6} and 8.0×10^{-4} Torr. In comparison, the groove/external surface sites lose less than $\frac{1}{5}$ of their original CO₂ population by

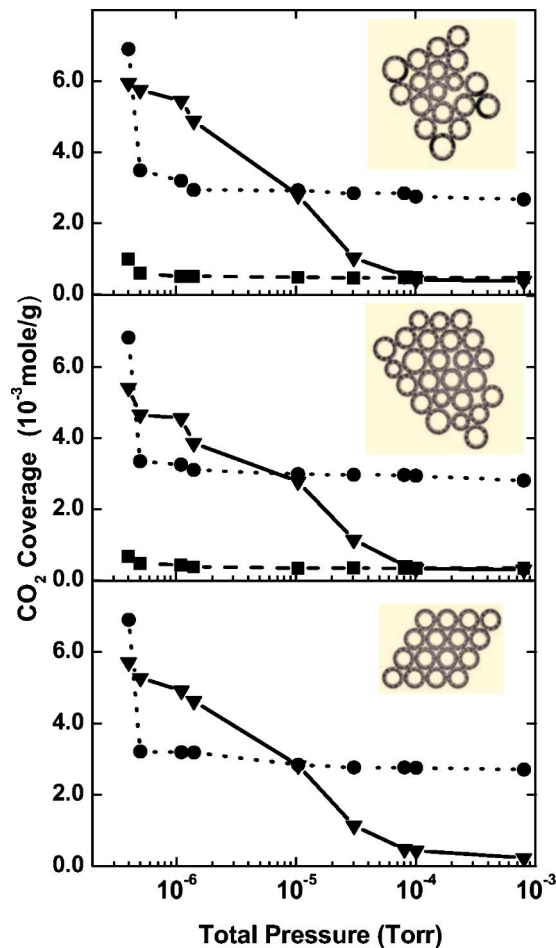


FIG. 3. GCMC simulation results for the coverage of CO_2 molecules in the endohedral (dotted lines and circles), interstitial (dashed lines and squares), and groove/external surface sites (solid lines and triangles) as a function of increasing Xe partial pressure. The CO_2 pressure is 7.0×10^{-7} Torr: (top) on heterogeneous bundle 1; (middle) on heterogeneous bundle 2; (bottom) on homogeneous bundle 3. The tubes making up these bundles are described in Table I and their cross-sections are illustrated in the insets.

1.7×10^{-6} Torr with the remaining fraction decreasing by slightly more than a factor of 10 by 8.0×10^{-4} Torr.

For each adsorption site there is some fraction of CO_2 molecules that are not easily displaced by Xe at the highest pressures studied. For the endohedral and interstitial sites this remaining fraction is slightly less than $\frac{1}{2}$ of the starting

CO_2 population with the groove/external surface sites retaining only $\sim \frac{1}{15}$ of their initial population. The reason for this remaining fraction of CO_2 can be explained by considering the average energy of the physisorbed CO_2 in each of the sites on the bundle (Table II). The endohedral and interstitial sites have the highest total average energies of 318.8 and 339.3 meV, respectively. In comparison, the groove and external surface sites have lower average energies of 258.5 and 252.2 meV, respectively. The total energy includes both CO_2 - CO_2 and CO_2 -SWNT interaction energies. The CO_2 - CO_2 interaction is a sum of the van der Waals (Lennard-Jones) and the quadrupole-quadrupole (coulombic) terms. Table II shows that the endohedral and interstitial sites are more strongly bound than groove and external surface sites and Xe will have more difficulty in displacing the more strongly bound species. The energies in Table II are average energies indicating that the fraction of CO_2 that is displaced from the endohedral and interstitial sites is likely from the lower end of the energy distribution associated with these sites. One interesting result in Table II is no single component of the average energy dominates the total energy trends seen in the different sites. The sum of all the components seems to be important when evaluating the relative stability of the different sites at the pressure and temperature used for the simulations. The importance of this observation is that one cannot predict displacement orders by the zero coverage solid-fluid energies only.

A representative IR experiment for the displacement of CO_2 by Xe at 77 K is shown for the SWNTs after heating to 700 K (Fig. 4). An initial decrease of intensity at 2330 cm^{-1} with subsequent loss of the 2340 cm^{-1} shoulder is seen. Results for bundles that have only been degassed at 373 K prior to use are similar, but with the contribution at 2330 cm^{-1} being far less pronounced.

The intensity changes associated with these CO_2 displacement experiments are best illustrated by subtracting the initial spectrum for the physisorbed CO_2 (no Xe present) from subsequent spectra as Xe is introduced into the cell (difference spectrum). Figure 5(a) shows difference spectra for the SWNT sample after degassing at 373 K. These difference spectra show that the introduction of Xe creates an initial intensity loss near 2330 cm^{-1} with a small shoulder at 2340 cm^{-1} . At higher pressures, a broad feature at 2340 cm^{-1} becomes evident. The initial loss near 2230 cm^{-1} indicates that some of the endohedral sites are open for CO_2 adsorption, although this is not obvious from the spectra of Fig. 1.

TABLE II. Average energies from canonical simulations for CO_2 at 7.0×10^{-7} Torr and 77 K as determined for bundle 2 of Table I.

Site	Total average energy (meV)	Solid-fluid energy (meV)	Fluid-fluid Lennard-Jones energy (meV)	Fluid-fluid Coulombic energy (meV)
Endohedral	318.8	218.6	65.2	35.0
Interstitial	339.3	277.0	42.3	20.0
Groove	258.5	235.1	8.7	14.7
Exterior surface	252.2	153.0	57.0	42.2

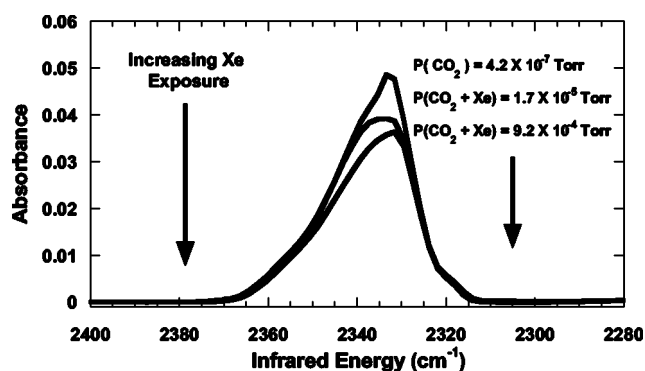


FIG. 4. Representative IR experiments of Xe displacement at 77 K on a SWNT sample after vacuum heating to 700 K. The sample cell is initially charged with 4.2×10^{-7} Torr before introducing Xe. Xe exposure causes an initial loss of intensity at 2330 cm^{-1} with loss of intensity at 2340 cm^{-1} at higher pressures. For clarity only three pressures are shown from the experiment.

To correlate the IR experiments of Fig. 5(a) with the molecular simulations we have used the data from the top panel of Fig. 3 (bundle 1) to carry out spectral simulations (see Sec. II). The results for a bundle with only 5% of the endohedral and interstitial sites open for adsorption are shown in Fig. 5(b). The spectral simulations in Fig. 5(b) show the same qualitative behavior as the experiments in Fig. 5(a). In the spectral simulations, the intensity loss at 2330 cm^{-1} occurs from the initial displacement of CO₂ in endohedral sites. Most of the initial intensity loss at 2340 cm^{-1} occurs from the partial displacement of groove/external surface site CO₂ occurring up to 1.70×10^{-6} Torr with the peak at 2339 cm^{-1} from interstitial CO₂ making a minor contribution overall. The large intensity loss centered at 2340 cm^{-1} dominating the spectral simulations at pressures above 10^{-5} Torr is mostly due to the displacement of groove/external surface site CO₂.

The qualitative behavior of the experimental and simulated spectra agrees rather well. The intensity loss for each peak occurs in the same relative order and over the same general pressure ranges. The fact that the intensity changes of the experimental spectra are well represented in the simulations of Fig. 5(b) by assuming that only 5% of the endohedral sites are open for CO₂ adsorption and displacement indicates that these sites are indeed mostly blocked by functionalization with the small open fraction causing the changes seen at 2330 cm^{-1} at low pressures. The fact that only a fraction of sites are open for endohedral adsorption could be a result of slight defunctionalization during the 373 K degassing step. Another possibility is that a small number of nanotubes have very large sidewall defects that allow for endohedral adsorption even though the defect peripheries are decorated with functional groups. As discussed in the Sec. II, the 5% scaling factor is only intended to illustrate how the selective blocking of these endohedral sites might affect the IR spectra and is not a quantitative representation of the actual number of opened endohedral sites.

The difference spectra for CO₂ displacement by Xe on the SWNTs heated to 700 K are shown in Fig. 6(a). An initial loss of intensity is seen at $\sim 2330 \text{ cm}^{-1}$ with a shoulder at 2340 cm^{-1} becoming visible at 4.3×10^{-4} Torr. The same

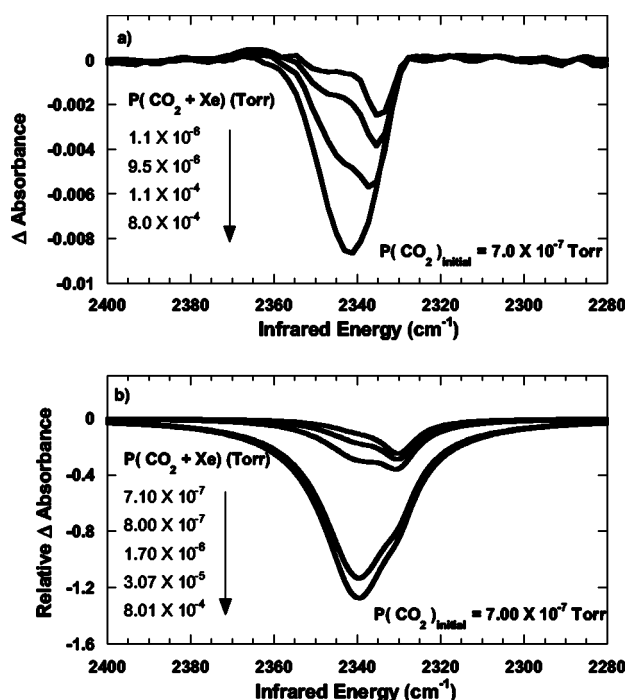


FIG. 5. (a) Experimental difference IR spectra for the displacement of CO₂ by Xe from the SWNT sample with an initial CO₂ pressure of 7.0×10^{-7} Torr. The sample has been degassed at 373 K and has most of its endohedral and interstitial sites blocked. (b) Simulated IR difference spectra derived from the GCMC results on a fully open heterogeneous bundle (bundle 1 of Table I) by scaling the endohedral and interstitial populations by 0.05 to mimic a bundle with only a small fraction of these sites available for adsorption and displacement. The initial CO₂ pressure in the simulation is 7.0×10^{-7} Torr.

sequence of intensity losses seen in Fig. 5(a) are observed except the overall intensity contributions differ, indicating that vacuum heating to 700 K has changed the accessibility of sites in the bundle. The spectral simulations for a fully open heterogeneous bundle are shown in Fig. 6(b). The simulations show an initial loss of intensity at 2330 cm^{-1} from displaced endohedral CO₂ followed by a loss at 2340 cm^{-1} from the displacement of groove/external surface site CO₂ starting at 1.07×10^{-5} Torr. Any loss of intensity at 2339 cm^{-1} occurring below 10^{-6} Torr in Fig. 6(b) from the displacement of interstitial CO₂ is obscured by the large changes seen for endohedral CO₂ at 2330 cm^{-1} . This occurs mainly because the interstitial species has an initial CO₂ population in the simulations that is $\sim \frac{1}{7}$ of the endohedral species. Overall, the spectral simulations reproduce the qualitative behavior of the displacement experiments rather well, indicating that the intensity losses seen experimentally are likely the result of CO₂ displacement from the sites indicated in the spectral simulations. Since all the bundles in Fig. 3 give nearly identical population profiles with pressure for endohedral and groove/external surface sites, we do not expect any significant differences by using these different bundle results in the spectral simulations.

As a control experiment, Xe displacement studies at 77 K were done without exposing the sample to CO₂ and after heating the sample to 700 K to test that the peaks at 2330

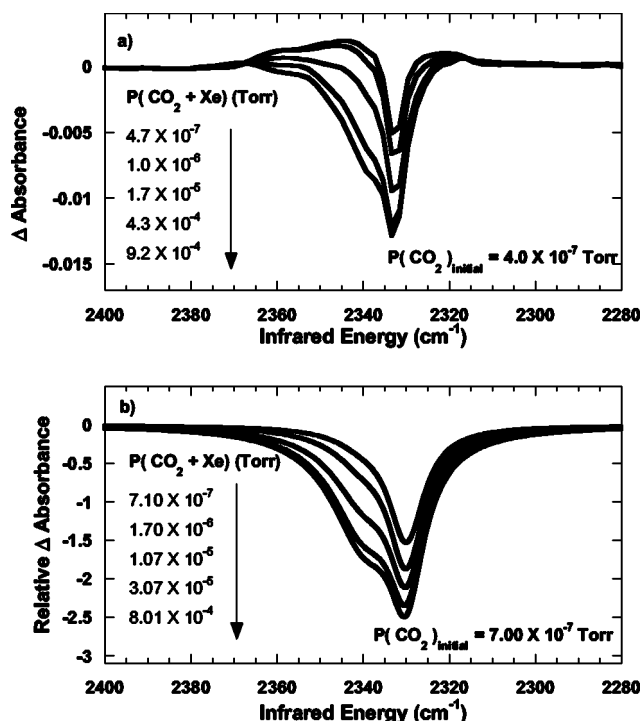


FIG. 6. (a) Experimental difference IR spectra for the displacement of CO_2 by Xe after vacuum heating the sample to 700 K. The experiment was run at 77 K with an initial CO_2 pressure of 4.0×10^{-7} Torr. (b) Simulated IR difference spectra from GCMC results on a fully open heterogeneous bundle (bundle 1 of Table I), which was used to mimic the vacuum heated sample used in the experiments shown in (a). The starting CO_2 pressure in the simulation is 7.00×10^{-7} Torr.

and 2340 cm^{-1} attributed to permanently entrapped CO_2 are not displaceable. No intensity changes for these peaks are seen up to Xe pressures of 9.0×10^{-4} Torr. Since the peaks at 2330 and 2340 cm^{-1} from the trapped CO_2 do not go away after exhaustive temperature cycles up to 700 K and venting to room air, they also are not expected to be displaced by gas phase Xe.^{4,7}

We do not expect quantitative agreement between the simulations and experiments for the relative amount of CO_2 displaced by Xe without a precise knowledge of the bundle size distribution in the experiments. This stems from the simple observation that the ratio of endohedral and interstitial sites to groove/external surface sites is not constant with bundle size. We can illustrate this effect if we approximate the bundle as a simple cylinder. The sum of endohedral and interstitial sites should be proportional to the cylinder volume and the number of groove/external surface sites to the surface area along the length of the cylinder. This means that bigger bundles will have a larger ratio of endohedral and interstitial sites to groove/external surface sites with this ratio scaling approximately as the radius of the cylinder. This effect is likely why we see IR peaks displaced in the same relative order in the simulations and experiments but with slightly different intensity contributions at each pressure.

The spectral and GCMC simulations suggest that most of the experimental intensity changes seen during Xe displacement of CO_2 occur because of population changes in endohe-

dral and groove/external surface sites. The large number of these sites with respect to interstitial sites in the simulation coupled with the qualitative agreement between simulations and experiments could lead to the conclusion that the interstitial sites play an insignificant role in this system. We urge caution with this interpretation. We do see a peak at 2339 cm^{-1} (Fig. 2) for trapped CO_2 , which we have attributed in the past to an interstitial species.⁴ The IR intensity ratio of trapped endohedral (2330 cm^{-1}) to trapped interstitial (2339 cm^{-1}) CO_2 in Fig. 2 is ~ 1.8 , which is obtained by fitting this spectrum to a 2 Lorentzian lineshape. This suggests a similar trapped CO_2 population ratio assuming the IR cross section for the molecule in each site is roughly the same. We cannot say conclusively that this ratio mirrors the ultimate CO_2 capacity for these sites but it does suggest that the interstitial sites could have a significant adsorption volume in the experimental system if it were completely accessible by a gas phase species. The remaining functionalities on the sample may play a role in inhibiting access.

The role that interstitial sites play in gas interactions with SWNTs will likely be very dependent on the sample's tube size distribution and processing history. A more homogeneous distribution of tubes will likely crystallize into bundles with smaller and more regular interstitial spaces that do not admit CO_2 . Thermal annealing may also affect how the tubes pack to form bundles and interstitial sites if this step causes a large decomposition of functionalities introduced in interstitial sites between the tubes during purification. Evidence in the literature has been found both for and against interstitial adsorption with no clear cut trend with molecular size or properties.^{3,4,7,8,22,23} It is possible that some of the variations seen regarding interstitial accessibility are largely due to differences in the samples used for these experiments.

IV. SUMMARY

The displacement of CO_2 by Xe on SWNTs has been investigated with IR spectroscopy and GCMC simulations. The experiments and simulations both show a sequential displacement of CO_2 with species associated with endohedral sites preceding those in groove/external surface sites. Slightly less than $\frac{1}{2}$ of the initial physisorbed CO_2 in interstitial and endohedral sites is not easily displaced by Xe whereas only $\frac{1}{15}$ of the CO_2 population is retained in groove/external surface sites at the same pressure and temperature. Spectral simulations constructed from the GCMC results qualitatively reproduce the IR experiments for the displacement of CO_2 by Xe. The agreement between the simulations and experiments suggests that the sites associated with each IR peak and their intensity changes with Xe exposure are indeed the result of CO_2 being displaced from the adsorption sites indicated by the GCMC simulations.

ACKNOWLEDGMENTS

We thank Milton Smith and Ed Bittner for useful discussions. Reference in this work to any specific product is to facilitate understanding and does not necessarily imply endorsement by the United States Department of Energy.

*Electronic address: matranga@netl.doe.gov

- ¹O. Byl, P. Kondratyuk, S. Forth, S. Fitzgerald, and J. T. Yates, *J. Am. Chem. Soc.* **125**, 5889 (2003).
- ²O. Byl, P. Kondratyuk, and J. T. Yates, *J. Phys. Chem. B* **107**, 4277 (2003).
- ³W. Yim, O. Byl, J. T. Yates, and J. K. Johnson, *J. Chem. Phys.* **120**, 5377 (2004).
- ⁴C. Matranga, L. Chen, M. Smith, E. Bittner, J. K. Johnson, and B. Bockrath, *J. Phys. Chem. B* **107**, 12930 (2003).
- ⁵M. Folman, M. Fastow, and Y. Kozirovski, *Langmuir* **13**, 1118 (1997).
- ⁶A. Lubezky, L. Chechelnitzsky, and M. Folman, *Surf. Sci.* **454**, 147 (2000).
- ⁷C. Matranga and B. Bockrath, *J. Phys. Chem. B* **108**, 6170 (2004).
- ⁸A. Kleinhammes, S. Mao, X. Yang, X. Tang, H. Shimoda, J. Lu, O. Zhou, and Y. Wu, *Phys. Rev. B* **68**, 075418 (2003).
- ⁹M. Cinke, J. Li, C. Bauschlicher, A. Ricca, and M. Meyyappan, *Chem. Phys. Lett.* **376**, 761 (2003).
- ¹⁰J. Zhao, A. Buldum, A. Han, and J. Lu, *Nanotechnology* **13**, 195 (2002).
- ¹¹M. Arab, F. Picaud, M. Devel, C. Ramseyer, and C. Girardet, *Phys. Rev. B* **69**, 165401 (2004).
- ¹²A. Thess, R. Lee, P. Nikolaev, H. Dai, P. Petit, J. Robert, C. Xu, Y. Lee, S. Kim, A. Rinzler, D. Colbert, G. Scuseria, D. Tomaneck, J. Fischer, and R. Smalley, *Science* **273**, 483 (1996).
- ¹³A. G. Rinzler, J. Liu, H. Dai, P. Nikolaev, C. Huffman, F. Rodriguez-Macias, P. Boul, A. Lu, D. Heymann, D. Colbert, R. Lee, J. Fischer, A. Rao, P. Eklund, and R. Smalley, *Appl. Phys. A: Mater. Sci. Process.* **67**, 29 (1998).
- ¹⁴J. Liu, A. Rinzler, H. Dai, J. Hafner, R. K. Bradley, P. Boul, A. Lu, T. Iverson, K. Shelimov, C. B. Huffman, F. Rodriguez-Macias, Y. Shon, T. R. Lee, D. Colbert, and R. E. Smalley, *Science* **280**, 1253 (1998).
- ¹⁵M. P. Allen and D. J. Tildesley, *Computer Simulation of Liquids* (Clarendon, Oxford, 1987).
- ¹⁶R. L. Rowley, *Statistical Mechanics for Thermophysical Property Calculations* (Prentice-Hall, Englewood Cliffs, NJ, 1994).
- ¹⁷J. G. Harris and K. H. Yung, *J. Phys. Chem.* **99**, 12021 (1995).
- ¹⁸W. A. Steele, *Surf. Sci.* **36**, 317 (1973).
- ¹⁹W. Shi and J. K. Johnson, *Phys. Rev. Lett.* **91**, 015504 (2003).
- ²⁰A. Kuznetsova, D. B. Mawhinney, V. Naumenko, J. T. Yates, J. Liu, and R. E. Smalley, *Chem. Phys. Lett.* **321**, 292 (2000).
- ²¹A. Kuznetsova, J. T. Yates, V. V. Simonyan, J. K. Johnson, C. B. Huffman, and R. E. Smalley, *J. Chem. Phys.* **115**, 6691 (2001).
- ²²W. Du, L. Wilson, J. Ripmeester, R. Dutrisac, B. Simard, and S. Denommee, *Nano Lett.* **2**, 343 (2002).
- ²³K. A. Williams, K. P. Bhabendra, P. C. Eklund, M. K. Kostov, and M. W. Cole, *Phys. Rev. Lett.* **88**, 165502 (2002).